Improving the Restorability of Bulk Power Systems with the Implementation of a WF-BESS System

Lei Sun, Weijia Liu, C. Y. Chung, *Fellow IEEE*, Ming Ding, Rui Bi, and Linjie Wang

***Abstract*—This paper proposes a restorability improvement strategy to accelerate system restoration through the implementation of a wind farm-battery energy storage system (WF-BESS) system. The concept of restorability is introduced and a restorability improvement model (RIM) is proposed and formulated as a mixed integer linear programming problem. To simulate the cylinder temperature drop during outages, the cranking time of a unit is modeled as a stepwise function of its startup time in the RIM. The WF might fail to meet its scheduled generation outputs optimized by the RIM due to the intermittency of wind. To tackle this problem, a linearized control strategy for the BESS (CSBESS) is proposed to minimize the difference between the scheduled wind power outputs and the combined power of the WF-BESS system. An iterative method is employed to efficiently solve the RIM and CSBESS by introducing optimality cuts. An actual power system case is employed to illustrate the effective performance of the proposed approach.**

***Index Terms*—Power system restoration, restorability, startup sequence, battery energy storage system, wind farm, resilience.**

NOMENCLATURE

Set:

Ω_G	Set of units.
Ω_S	Set of scenarios.

Parameters:

E^{b}_{cap}	Energy capacity of the BESS.
E^{b}_{min}	Allowed minimum energy of the BESS.
E^{b}_{max}	Allowed maximum energy of the BESS.
E^{min}_{w}	Minimum wind energy generation of typical scenarios in the restoration period.
E^{max}_{w}	Maximum wind energy generation of typical scenarios in the restoration period.
M	A constant with big value.
N_K	Number of states a unit goes through after an outage.
P^{max}_{g}	Maximum power output of unit g.
P^{st}_{g}	Cranking power of unit g.
p^{ch}_{max}	Maximum charging power of the BESS.
p^{disch}_{max}	Maximum discharging power of the BESS.
P^{w}_{rated}	Rated power outputs of the WF.
$P^{w,min}_{t}$	Minimum wind output of typical scenarios at time t.
$P^{w,max}_{t}$	Maximum wind output of typical scenarios at time t.
$\hat{P}^{w,sch}_{t}$	Scheduled wind power output solution of the RIM at time t.
P^{+}_{wr}	Power increase rate limit of the WF.
P^{-}_{wr}	Power decrease rate limit of the WF.
$P^{w}_{t,s}$	Wind power outputs at time t in scenario s.
P_{load}	Power demands of all loads.
P_{rev}	Reserve power of the power system.
P_{loss}	Power losses of the power system.
R_g	Ramping rate of unit g.
$t^{c,k}_{g}$	Cranking time of unit g in state k, where $k = 1...N_K$.
t^{k}_{g}	The k^{th} separation point of restarting states of unit g.
t_{st}	Starting time of the power system restoration period.
T	Restoration time horizon, which equals t_{end} minus t_{st}.
T_G	Number of time intervals in the RIM.
T_B	Number of time intervals in the CSBESS.
T^{max}_{g}	Critical maximum time interval for start of unit g.
T^{min}_{g}	Critical minimum time interval for start of unit g.
U^{ch}_{min}	Minimum continuous charge time of the BESS.
U^{disch}_{min}	Minimum continuous discharge time of the BESS.
U^{ch}_{0}	Number of time intervals the BESS has been charging at the beginning of the restoration horizon.
U^{disch}_{0}	Number of time intervals the BESS has been discharging at the beginning of the restoration horizon.
V_T	Length of each time interval in the RIM.
V_B	Length of each time interval in the CSBESS.
η	Coefficient of charge/discharge efficiency.
γ	Fluctuation restriction.
τ	Penalty cost.
β	Tolerance threshold for the difference between the scheduled wind power and the combined power of the WF-BESS system.
κ	Initial state of charge of the BESS.

Variables:

C_g	Generation capability of unit g in the restoration time horizon.
$C_{g,1}$	Generation capability of unit g if the unit reaches its maximum power output at t_{end}.
$C_{g,2}$	Generation capability of unit g if the unit is ramping up at t_{end}.
$E^{b}_{t,s}$	Energy of the BESS in scenario s at time t.
$P_{g,t}$	Active power output of unit g at time t.
$P^{ab}_{t,s}$	Abandoned wind power in scenario s at time t.
$P^{st}_{g,t}$	Cranking power of unit g at time t.
P^{b}_{t}	Active power output of the BESS at time t.

This work is supported by the National Key R&D Program of China (No. 2016YFB0900400), the Postdoctoral Innovation Talent Support Program of China (No. BX201700211) and the Fundamental Research Funds for the Central Universities (No. JZ2018HGTA0213).

L. Sun, M. Ding and R. Bi are all with the School of Electrical Engineering and Automation, Hefei University of Technology, Hefei 230009, China (Email: leisun@hfut.edu.cn; mingding56@126.com; biruizz@126.com)

W. Liu and C. Y. Chung are with the Department of Electrical and Computer Engineering, University of Saskatchewan, Saskatoon, SK S7N 5A9, Canada. (Email: liuweijiamarcel@gmail.com; c.y.chung@usask.ca)

L. Wang is with State Grid Zhejiang Shaoxing Shangyu Power Supply co, LTD, Shaoxing 312300, China (Email: 540995062@qq.com).

$P_{t,s}^{\mathrm{b}}$	Active power output of the BESS in scenario s at time t.
P_t^{ch}	Charging power of the BESS at time t.
$P_{t,s}^{\mathrm{ch}}$	Charging power of the BESS in scenario s at time t.
P_t^{disch}	Discharging power of the BESS at time t.
$P_{t,s}^{\mathrm{disch}}$	Discharging power of the BESS in scenario s at time t.
P_t^{w}	Active power output of the WF at time t.
P_t^{wb}	Combined power of the WF-BESS system at time t.
$P_{t,s}^{\mathrm{wb}}$	Combined power of the WF-BESS system in scenario s at time t.
$P_t^{\mathrm{w,sch}}$	Scheduled wind power output at time t.
$P_{t,s}^{\mathrm{w,sch}}$	Scheduled wind power output in scenario s at time t.
R_c	Restorability of a power system after an outage.
t_{end}	Ending time of the power system restoration period.
t_g^{st}	Starting time of unit g.
t_g^{c}	Cranking time of unit g to begin to parallel with a power system.
$T_{g,h',t}^{\mathrm{au,c}}$	The h' th auxiliary variable representing the cranking time of unit g at time t, where h' is 1, 2.
$\mathbf{T}_{\mathrm{B}}, \mathbf{T}_{\mathrm{L}}, \mathbf{T}^{\mathrm{st}}$	Restoration time vector of buses, lines, and units.
$u_{t,s}^{\mathrm{ch}}, u_{t,s}^{\mathrm{disch}}$	Charge and discharge state in scenario s at time t.
$v_{g,h,t}$	Auxiliary variable in the RIM.
W_s	Penalty in scenario s.
$w_{g,h,t}$	The h^{th} auxiliary binary variable representing the restoration status of unit g at time t.
$\psi_{t,s}, \varpi_{t,s}$	Auxiliary variables introduced to eliminate the absolute operation in the CSBESS.
$y_{t,s}^{\mathrm{ch}}$	0/1 variable, equal to 1 if the BESS starts to charge in scenario s at time t.
$y_{t,s}^{\mathrm{disch}}$	0/1 variable, equal to 1 if the BESS starts to discharge in scenario s at time t.
z_g	Binary variable, equal to 1 if unit g reaches its maximum power output at t_{end} and 0 if it is still ramping at t_{end}.
$\lambda_{t,s}$	Multiplier of constraint (60) (dual variable)
δ_g^k	Binary variable, equal to 1 if unit g goes through the k^{th} state before being started and 0 otherwise.

I. INTRODUCTION

THE increasing number of extreme weather events and cyber attacks in recent years has made power system outages occur more frequently than ever before. For example, Ukrainian power companies were attacked by false data injection on 23 December 2015, sending approximately 225,000 customers into darkness [1]. On 6 September 2016, a blackout event occurred due to lightning strikes in the northeast British Columbia Hydro system [2]. The South Australia power system with high renewable penetration experienced a major outage because of a severe storm in 2016, which led to a power shortage for about 1,700,000 people and caused an economic loss of around \$367 million Australian dollars [3]. In summary, outages have significant negative impacts on the economy and society, and those impacts grow exponentially with increased outage time. A fast and reliable restoration planning strategy is helpful to reduce outage time and accelerate the speed of power system restoration. Therefore, a reasonable restoration planning strategy is urgently needed, especially for modern power systems characterized by high penetration of renewable energy resources. If not handled properly, the volatility, intermittency, and uncertainty introduced by the renewable energy resources can prolong the restoration procedure or even lead to critical restoration failures [4]. Wind power, as an important pollution-free renewable energy resource, has been increasingly installed worldwide in recent years [5]. However, the growing penetration of wind power affects many aspects of power system operation, including power system restoration after a blackout. Therefore, investigating the role of wind power in power system restoration is necessary.

Restoration planning for the conventional power systems has been well studied in existing literature [6]-[8]. With the growing integration of wind power into power systems, some researchers have noted the possible role of wind energy in accelerating restoration speed. In [4], the control strategies for restarting Type 3 wind turbines and starting a local power system by deploying Type 3 wind turbines are proposed. Battery rating is discussed to meet the power balance requirement. System frequency stability can be maintained by the control strategy for Type 3 wind turbines and the impact of control parameters on the frequency response is assessed. Reference [9] proposes a two-stage adaptive robust coordination strategy of wind and pumped-storage hydro units for system restoration. The results show that the load pickup capability can be improved by storing/releasing wind energy with the aid of pumped-storage hydro units. Reference [10] proposes a restoration planning tool considering the participation of wind energy. To handle the uncertainty of wind power, the proposed model is expressed as a stochastic programming model and solved by the L-shaped method. Reference [11] investigates the black start participation of a doubly-fed induction generator based wind turbine and proposes a control strategy for the associated energy storage system. The results verify the black start capability of the doubly-fed induction generator based wind turbine with a battery energy storage system (BESS), where the wind turbine provides active and reactive power and the BESS is employed to minimize power imbalance and maintain the load voltages through the converters. In [12], the restoration sequence of generation units and loads is optimized by a dynamic programming method, assuming that the power outputs of wind farms (WFs) are relatively stable. Reference [13] proposes a robust optimization model to maximize the dispatched power of WFs at the beginning of the power system restoration process. In most existing studies, the wind power takes part in the power system restoration in a passive way. The uncertain wind power outputs are regarded as parameters (e.g., negative uncontrollable loads) in existing restoration models. As a result, the optimized restoration strategies must sacrifice restoration speed to accommodate wind power fluctuations. Worse yet is that the intermittency of wind may also result in restoration failures.

To improve the utilization efficiency of wind power, integrating a BESS into a WF has been shown to be an efficient solution [14]. The role of BESSs can be generally described as: 1) smoothing the power outputs of WFs [15]-[16]; 2) meeting the scheduled power outputs of WFs [17]; and 3) improving the ancillary service capacity of WFs [18]-[19], including peak shaving, automatic generation control, and black start service. Experts have investigated the implementation of a WF-BESS system in areas including but not limited to [19]-[22]: 1) automatic generation control; 2) power system operation cost reduction; 3) power system reliability and power quality enhancement; 4) voltage profile improvement; and 5) peak shaving. However, the application of a WF-BESS in power system restoration has not been well investigated. With the aid of a BESS to level off the output fluctuations, the wind power is able to produce sustainable and reliable power generation and takes part in power system restoration in a positive way. Thus, the implementation of a WF-BESS system in accelerating power system restoration speed is one of the main contributions of this paper.

When a blackout occurs, the non-black-start units (NBSUs) cannot be restarted until they receive cranking power supplied by the black-start unit (BSU). As the outage time increases, the cylinder temperature of an NBSU gradually decreases which means more time is needed for the corresponding NBSU to restart. The cranking time of the NBSU, which greatly impacts the restoration process, depends on the profile of its cylinder temperature. In existing works, the cranking time of an NBSU is generally assumed to be constant for simplification; therefore, the drop in cylinder temperature is ignored during the entire power system restoration process. However, this simplification may result in over-optimistic, or even infeasible restoration strategies. On the other hand, modeling the detailed mathematical function of the cranking time and cylinder temperature is difficult. In this work the cranking time is modeled as a stepwise function of the outage time, taking the cylinder temperature drop into account.

This paper proposes a restorability improvement strategy for power systems with a WF-BESS system. Compared to existing works, the proposed method aims to integrate the WF-BESS system into power system restoration planning models and employ the positive role of the WF-BESS system to accelerate the restoration procedure. The concept of restorability is defined as the generation capability during the restoration period divided by the restoration time, and a restorability improvement model (RIM) is proposed to maximize the restorability for the purpose of improving the resilience of power systems. The cranking time of NBSUs is formulated as a stepwise function of their outage time considering the relationship between cranking time and cylinder temperature. By employing the linearization method, the proposed RIM is expressed as a mixed integer linear programming (MILP) problem. Typical wind power generation scenarios are generated and reduced to model the uncertainty of wind power outputs, and a control strategy for the BESS (CSBESS) is proposed to ensure the power outputs of the WF-BESS system can meet the scheduled wind power optimized by the RIM. If the difference between the scheduled wind power and the combined power of the WF-BESS system exceeds a given threshold, a cut will be generated and added to the RIM. The RIM and CSBESS are solved iteratively until the termination criterion is reached. The contributions of this paper are summarized as follows:

1) The concept of power system restorability is defined and a restorability improvement model is proposed. In addition to the maximization of generation capability that has been widely considered in existing work, the proposed RIM also investigates the impacts of the length of restoration period on the restoration planning results, which had not yet been properly studied.
2) The generation capability during the restoration period is modeled more accurately compared to existing studies. Instead of relying on fixed cranking times and installed capacities of NBSUs, the proposed method models the time-varying characteristics of NBSU cranking times and integrates comprehensive features of NBSUs, such as ramping status, to enhance the accuracy of generation capability modeling.
3) The role of the WF-BESS system in accelerating the power system restoration process is studied and an optimal control strategy for the BESS is developed to operate the BESS during the restoration period.
4) Linearized methods are employed to formulate the RIM and CSBESS as MILPs, which can be efficiently solved by commercial solvers. To reduce the computational burden, an iterative solution strategy is employed to solve the proposed models by generating cuts.

The remainder of this paper is organized as follows. Section II describes the WF-BESS system as well as the system restoration strategy considering the WF-BESS system. Section III introduces the definition of restorability and proposes the RIM. Section IV presents the CSBESS. Section V presents the solution method. Section VI presents the simulation results. Section VII presents conclusions of the work.

II. System Restoration Strategy Considering the WF-BESS System

A. System Description

In this work, the WF-BESS system is comprised of a WF and a BESS, as shown in Fig. 1. The wind energy is converted into electrical power in a WF, the power output of which is determined by conditions and profiles of on-site wind. In this paper, a BESS with a fast response and exhibiting high performance is deployed to enhance the flexibility of the WF. The BESS is designated to compensate for output fluctuations of a WF and ensure the wind power can exactly meet the scheduled power. The power output of the BESS at time *t* can be expressed as

$$P_t^{\mathrm{b}}=P_t^{\mathrm{disch}}-P_t^{\mathrm{ch}} \tag{1}$$

If P_t^{b} is positive, the BESS is supposed to be discharged; otherwise, the BESS should be charged. The assumed direction of power flows is denoted by the arrows in Fig.1.

The combined power output of the WF-BESS system is the sum of the power output of the WF and that of the BESS, which can be expressed as

$$P_t^{\mathrm{wb}}=P_t^{\mathrm{b}}+P_t^{\mathrm{w}} \tag{2}$$

In this work, the Latin hypercube sampling method [23] is applied to generate a number of scenarios to describe the stochastic nature of wind power based on the Weibull distribution, and an efficient scenario reduction algorithm [24] is employed to produce a set of typical scenarios for the purpose of reducing the computational burden. Both the Latin hypercube sampling method and scenario reduction algorithm have been well studied and are beyond the scope of this paper, and therefore are not described in detail.

Note that the WF and BESS are generally connected to the main grid through the point of common coupling. Therefore, the WF and the BESS are usually placed close to each other [18], [25]-[26]. If the WF and the BESS are not placed close to each other, the BESS energizes the transmission lines that connect the BESS and the WF, and the WF can be restarted by the power supply from the BESS after an outage [4]. The BESS, WF and energized transmission path constitute a WF-BESS system. The focus of this paper is on investigating the role of WF-BESS systems in power system restoration and improving the restorability of power systems with the aid of the WF-BESS system. Therefore, selection of the energized transmission path and how to model the restart process of the storage are not discussed.

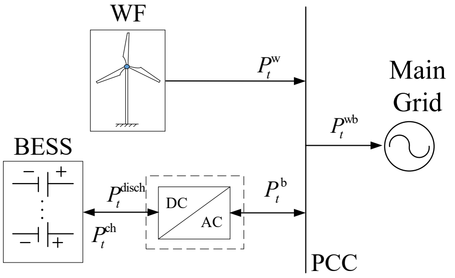

Fig. 1 Schematic of a typical integrated WF and BESS system.

B. System Restoration Strategy

After an outage, a system restoration strategy that consists of the restart of units, restoration of transmission lines, and load pickup is employed to bring the system back to a normal operating condition. This paper focuses on the first task of the restoration process, which aims to restart units. Some units can be started on their own without a power supply from the grid, and are called BSUs. Other units, called NBSUs, can only be started by receiving cranking power supplied by BSUs [10].

With the aid of a BESS, the outputs of a WF can be regarded as dispatchable with respect to certain limitations. The WF-BESS system can act as a black-start source to take part in the power system restoration. In our scheme, the available power of the WF-BESS system is taken into consideration in the system restoration strategy. The power outputs of a WF are scheduled by taking into consideration their role in accelerating the restart of units, which is carried out in the proposed RIM. The control method of the BESS is applied to ensure the actual power outputs of the WF-BESS system can meet the scheduled ones, and the objective of CSBESS is to minimize the difference between the scheduled wind power outputs and the combined power outputs of the WF-BESS system.

III. Restorability Improvement Model

A. Definition of Restorability

Restorability can be regarded as an important resilience index for a power system in the restorative state. According to the resilience metrics introduced in [27]-[28], restorability can be defined as the total generation capability throughout the restoration period divided by the length of the restoration period, which is given as:

$$R_{\mathrm{c}} = \frac{\sum_{g\in\Omega_{\mathrm{G}}} C_g}{T} \tag{3}$$

where T=t_{end}-t_{st}. To simplify the expression, the starting time t_{st} can be assumed as 0.

The power capability of a unit is related to its starting time, cranking power demand, cranking time, ramping rate, and maximal capacity. The detailed startup characteristics of unit g are shown in Fig. 2, where unit g is cranked at t_g^{st}, and after time t_g^{c} begins to ramp up and parallel with the power system. At time $t_g^{\mathrm{st}}+t_g^{\mathrm{c}}+P_g^{\mathrm{st}}/R_g$, the active power output of unit g is equal to its cranking power demand, and it is able to deliver active power to the system thereafter. During the restoration procedure of unit g (from t_{st} to t_{end}), if unit g reaches its maximal output at t_{end}, its generation capability is the area of the dark green region minus the area of the dark orange region in Fig. 2(a), which can be calculated as

$$\begin{aligned} C_{g,1} &= \frac{\left(P_g^{\max}\right)^2}{2R_g} + \left(t_{\mathrm{end}} - t_g^{\mathrm{st}} - t_g^{\mathrm{c}} - \frac{P_g^{\max}+P_g^{\mathrm{st}}}{R_g}\right)P_g^{\max} - \frac{1}{2}\left(t_g^{\mathrm{c}} + t_g^{\mathrm{c}} + \frac{P_g^{\mathrm{st}}}{R_g}\right)P_g^{\mathrm{st}} \\ &= \frac{-\left(P_g^{\max}+P_g^{\mathrm{st}}\right)^2}{2R_g} + P_g^{\max}T - t_g^{\mathrm{st}}P_g^{\max} - t_g^{\mathrm{c}}\left(P_g^{\max}+P_g^{\mathrm{st}}\right) \end{aligned} \tag{4}$$

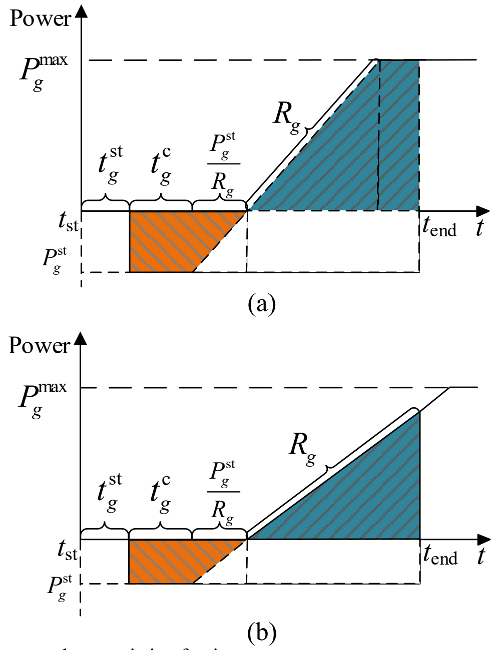

Fig. 2 Startup characteristic of unit g

If unit g is still ramping up at t_{end} as shown in Fig. 2(b), its generation capability is the area of the light green region minus the area of the dark orange region and is calculated as

$$\begin{aligned} C_{g,2} &= 0.5R_g\left(t_{\mathrm{end}} - t_g^{\mathrm{st}} - t_g^{\mathrm{c}} - P_g^{\mathrm{st}}/R_g\right)^2 - 0.5\left(t_g^{\mathrm{c}} + t_g^{\mathrm{c}} + P_g^{\mathrm{st}}/R_g\right)P_g^{\mathrm{st}} \\ &= 0.5R_g\left(t_g^{\mathrm{st}} + t_g^{\mathrm{c}}\right)^2 - \left(R_g t_{\mathrm{end}} - P_g^{\mathrm{st}}\right)t_g^{\mathrm{st}} - R_g t_{\mathrm{end}} t_g^{\mathrm{c}} + 0.5R_g t_{\mathrm{end}}^2 - t_{\mathrm{end}}P_g^{\mathrm{st}} \end{aligned} \tag{5}$$

Therefore, taking these two cases into account, the total generation capability during the restoration period can be expressed as

$$C_g = \begin{cases} C_{g,1} & t_{\mathrm{end}} \ge t_g^{\mathrm{st}} + t_g^{\mathrm{c}} + \left(P_g^{\max} + P_g^{\mathrm{st}}\right)/R_g \\ C_{g,2} & t_{\mathrm{end}} < t_g^{\mathrm{st}} + t_g^{\mathrm{c}} + \left(P_g^{\max} + P_g^{\mathrm{st}}\right)/R_g \end{cases} \tag{6}$$

B. Mathematical Model for Restorability Improvement

A mathematical model for restorability improvement is proposed in this subsection, with the objective of maximizing the restorability index, shown as:

$$\max\ R_{\mathrm{c}} \tag{7}$$

According to (3)-(6), the only variables in (7) are t_g^{st} and t_g^{c} once the starting time and ending time of the restoration procedure are fixed. Thus, (7) can be reformulated as:

$$\max \sum_{g\in\Omega_{\mathrm{G}}} C_g \tag{8}$$

$$-(1-z_g)M \le C_g - C_{g,1} \le (1-z_g)M \tag{9}$$

$$-z_g M \le C_g - C_{g,2} \le z_g M \tag{10}$$

$$(z_g\text{-}1)M \le t_{\mathrm{end}} - t_g^{\mathrm{st}} - t_g^{\mathrm{c}} - \left(P_g^{\max} + P_g^{\mathrm{st}}\right)/R_g \le z_g M \tag{11}$$

The quadratic part in $C_{g,2}$ can be linearized by piecewise linear approximation [29]. To secure the system restoration procedure, the following constraints should be met [9], [30].

1) Constraints of critical minimum and maximum time:

$$t_g^{\mathrm{st}} \ge T_g^{\min},\ \forall g \in \Omega_{\mathrm{G}} \tag{12}$$

$$t_g^{\mathrm{st}} \le T_g^{\max},\ \forall g \in \Omega_{\mathrm{G}} \tag{13}$$

Eqn. (12) shows that the starting time of unit g should be larger than its critical minimum time. Eqn. (13) indicates that the starting time of unit g should be smaller than its critical maximum time.

2) Constraints of start-up power requirement:

$$P_{t'}^{\mathrm{w,sch}} + \sum_{g\in\Omega_{\mathrm{G}}} (P_{g,t} - P_{g,t}^{\mathrm{st}}) \ge 0, \forall t = 1,..,T_{\mathrm{G}}, t' = tV_{\mathrm{B}} / V_{\mathrm{T}} \tag{14}$$

If the cranking time of a unit is constant, (14) can be linearized by the method proposed in [31]. However, as the outage time increases, the cylinder temperature decreases and thus a unit requires more time to restart. In this paper, units are divided into four restarting states: extremely hot start-up, hot start-up, warm start-up, and cold start-up [32]. The lower the cylinder temperature, the longer the cranking time. For simplicity, the cranking time of a unit at each stage is assumed to be constant, as shown in Fig. 3. Therefore, the cranking time of unit g can be expressed as

$$t_g^{\mathrm{c}} = \delta_g^1 t_g^{c,1} + \sum_{k=2}^{N_K} \delta_g^k \left(t_g^{c,k} \text{-} t_g^{c,k\text{-}1} \right) \tag{15}$$

$$\delta_g^1 = 1 \tag{16}$$

$$-(1-\delta_g^k)M \le t_g^{\mathrm{st}} - t_g^{k-1} \le \delta_g^k M, k \in [2,..,N_K] \tag{17}$$

The accuracy of this stepwise approximation can be easily enhanced by increasing the number of steps according to the characteristics of the units, but this is not further discussed herein.

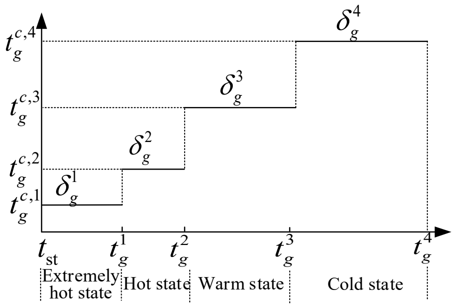

Fig. 3 Cranking time of units in different states (N_K=4)

The critical minimum and maximum time constraints (12) and (13) can be relaxed by setting proper parameters according to Fig. 3, for the following reasons.

1) The value of $t_g^{c,1}$ for unit g with minimum time constraints can be set as a large value, and the value of t_g^1 is set as the minimum startup time. In this way, the optimal startup time of unit g will be larger than its minimum startup time.

2) The value of $t_g^{c,4}$ for unit g with maximum time constraints can be set as a large value, and the value of t_g^3 is set as the maximum startup time. In this way, the optimal startup time of unit g will be less than its maximum startup time.

By introducing a new variable $T_{g,h',t}^{\mathrm{au,c}}$ and employing the method in [31], the start-up power requirement can be shown as

$$\sum_{g\in\Omega^{\mathrm{G}}} (-v_{g,1,t} R_g V_{\mathrm{T}} + w_{g,1,t} t V_{\mathrm{T}} R_g \text{-} T_{g,1,t}^{\mathrm{au,c}} R_g + w_{g,2,t} P_g^{\max} - w_{g,3,t} P_g^{\mathrm{st}}) + P_{t'}^{\mathrm{w,sch}} \ge 0,\quad t' = tV_{\mathrm{B}} / V_{\mathrm{T}} \tag{18}$$

The introduced auxiliary variables $w_{g,h,t}$ and $v_{g,h,t}$ (where h = 1,2,3) respect the following constraints:

$$0 \le w_{g,1,t} + w_{g,2,t} \le 1, \quad \forall g \in \Omega_{\mathrm{G}} \tag{19}$$

$$t\left(w_{g,1,t} + w_{g,2,t} \right) \ge t - t_g^{\mathrm{st}} \text{-} t_g^{\mathrm{c}}, \quad \forall g \in \Omega_{\mathrm{G}} \tag{20}$$

$$v_{g,1,t} + T_{g,1,t}^{\mathrm{au,c}} \le t, \quad \forall g \in \Omega_{\mathrm{G}} \tag{21}$$

$$v_{g,2,t} + T_{g,2,t}^{\mathrm{au,c}} + w_{g,2,t}\left(P_g^{\max} + P_g^{\mathrm{st}} \right) / R_g / V_{\mathrm{T}} \le t, \quad \forall g \in \Omega_{\mathrm{G}} \tag{22}$$

$$w_{g,1,t} \times t \le t_g^{\mathrm{st}} + t_g^{\mathrm{c}} + \left(P_g^{\max} + P_g^{\mathrm{st}} \right) / R_g / V_{\mathrm{T}}, \quad \forall g \in \Omega_{\mathrm{G}} \tag{23}$$

$$v_{g,3,t} \le t, \quad \forall g \in \Omega_{\mathrm{G}} \tag{24}$$

$$t w_{g,3,t} \ge t - t_g^{\mathrm{st}}, \quad \forall g \in \Omega_{\mathrm{G}} \tag{25}$$

$$0 \le v_{g,h,t} \le w_{g,h,t} T_{\mathrm{G}}, \quad \forall g \in \Omega_{\mathrm{G}} \tag{26}$$

$$t_g^{\mathrm{st}} - (1 - w_{g,h,t}) T_{\mathrm{G}} \le v_{g,h,t} \le t_g^{\mathrm{st}} + (1 - w_{g,h,t}) T_{\mathrm{G}}, \forall g \in \Omega_{\mathrm{G}} \tag{27}$$

Eqn. (19) shows that unit g cannot keep ramping up and reach its maximum capacity at time t simultaneously. Eqn. (20) indicates that unit g either ramps up or reaches its maximum capacity at time t after $t_g^{\mathrm{st}} + t_g^{\mathrm{c}}$. Eqns. (21) and (22) show that unit g cannot ramp up and reach its maximum capacity before $t_g^{\mathrm{st}} + t_g^{\mathrm{c}}$ and $t_g^{\mathrm{st}} + t_g^{\mathrm{c}} + \left(P_g^{\max} + P_g^{\mathrm{st}} \right) / R_g$, respectively. Eqn. (23) forces that unit g cannot keep ramping up once the maximum capacity is reached. Eqns. (24)-(27) indicate that unit g cannot be restarted before t_g^{st}.

The variable $T_{g,h',t}^{\mathrm{au,c}}$ satisfies the condition that $T_{g,h',t}^{\mathrm{au,c}} = w_{g,h',t} t_g^{\mathrm{c}}$. By employing the big-M method, $T_{g,h',t}^{\mathrm{au,c}}$ can be linearized as

$$0 \le T_{g,h',t}^{\mathrm{au,c}} \le w_{g,h',t} M \tag{28}$$

$$-(1 - w_{g,h',t}) M \le T_{g,h',t}^{\mathrm{au,c}} - t_g^{\mathrm{c}} \le (1 - w_{g,h',t}) M \tag{29}$$

Eqns. (28) and (29) show that the variable $T_{g,h',t}^{\mathrm{au,c}}$ is equal to t_g^{c} if $w_{g,h',t}$ is 1, and 0 otherwise.

3) The restoration time constraints of lines, buses, and units are given by

$$\mathbf{G}(\mathbf{T}_{\mathrm{B}}, \mathbf{T}_{\mathrm{L}}, \mathbf{T}^{\mathrm{st}}) \le \mathbf{0} \tag{30}$$

Eqn. (30) shows the mathematic relationship of restoration time of lines, buses, and units, which is introduced in detail in [31].

4) The scheduled wind power output/energy limits [33] are given by

$$P_t^{\mathrm{w,min}} \le P_t^{\mathrm{w,sch}} \le P_t^{\mathrm{w,max}} \tag{31}$$

$$E_{\mathrm{w}}^{\min} \le \sum_{t=1}^{T_{\mathrm{G}}} P_t^{\mathrm{w,sch}} V_{\mathrm{T}} \le E_{\mathrm{w}}^{\max} \tag{32}$$

Eqns. (31) and (32) enforce that the scheduled wind power output at time t and scheduled wind energy are respectively between the upper and lower bounds.

5) The ramp rate limits of the scheduled wind power are given by

$$p_{\mathrm{wr}}^{-} \le P_t^{\mathrm{w,sch}} - P_{t-1}^{\mathrm{w,sch}} \le p_{\mathrm{wr}}^{+} \tag{33}$$

Eqn. (33) enforces that the ramp rate of the scheduled wind power is between the upper and lower bounds.

Moreover, the restoration constraints of a concerned line should also be considered in the proposed model, and this is introduced in [31] in detail. Note two major improvements in the model presented here compared to that in [31]. First, the model in this work takes into consideration the relationship between cranking time and starting time of units. In practice, the cranking time of units will be prolonged due to the increase in starting time in the actual system restoration process, and thus the proposed expanded model is more suitable for actual applications than [31], which assumes the cranking time of NBSUs is constant. Second, the proposed mathematical expression of the generation capability during the restoration period is more accurate, as both the units that have reached their maximum power output and those that are still ramping at the end of the restoration period are properly modeled.

To sum up, the RIM can be formulated as

$$\begin{aligned} &Obj.\ (8) \\ &s.t.\ (4)-(5),(9)-(13),(15)-(33) \end{aligned} \tag{34}$$

IV. Control Strategy for Energy Storage

Due to the intermittency and volatility of wind power, the actual wind power in the power restoration procedure might not be scheduled as optimized in Section III. As a powerful tool to address uncertainties [34], [35], the scenario analysis method is employed in this paper to cope with the uncertainties of wind power outputs.

In this section, a control strategy for the BESS is proposed to ensure the power output of the WF-BESS system matches the scheduled power obtained by the RIM (34). A small difference is acceptable in most cases [36], and the objective function is constructed to minimize the penalty resulting from a large power difference between the scheduled wind power and the actual combined power of the WF-BESS system for each representative wind scenario *s*, which is expressed as

$$\min W_s = \sum_{t=1}^{T_\mathrm{B}} H(P_{t,s}^{\mathrm{wb}} - P_{t,s}^{\mathrm{w,sch}}) \tag{35}$$

where *H*() is the penalty function, which can be described as:

$$H(x) = \begin{cases} 0 & |x| \le \beta \\ \tau\left(|x| - \beta\right) & |x| > \beta \end{cases} \tag{36}$$

Note that (35) is compatible. If the value of β is reduced to 0, the objective is changed to minimize the difference between the scheduled wind power output and the power of the WF-BESS system.

However, the objective function in (35) is not convex, therefore making it difficult to solve effectively. To reduce computational burden, a linearization method is proposed and (35) can be reformulated as:

$$\min \sum_{t=1}^{T_\mathrm{B}} \tau \psi_{t,s} \tag{37}$$

$$\psi_{t,s}, \varpi_{t,s} \ge 0 \quad t = 1,2..,T_\mathrm{B},\, s \in \Omega_\mathrm{S} \tag{38}$$

$$\psi_{t,s} \ge \varpi_{t,s} - \beta \quad t = 1,2..,T_\mathrm{B}, s \in \Omega_\mathrm{S} \tag{39}$$

$$-\varpi_{t,s} \le P_{t,s}^{\mathrm{wb}} - P_{t,s}^{\mathrm{w,sch}} \le \varpi_{t,s} \quad t = 1,2..,T_\mathrm{B}, s \in \Omega_\mathrm{S} \tag{40}$$

The following constraints for each scenario *s* should be met.

1) Power limits of a BESS.

$$P_{t,s}^{\mathrm{b}} = P_{t,s}^{\mathrm{disch}} - P_{t,s}^{\mathrm{ch}} \tag{41}$$

$$0 \le P_{t,s}^{\mathrm{ch}} \le p_{\max}^{\mathrm{ch}} u_{t,s}^{\mathrm{ch}} \tag{42}$$

$$0 \le P_{t,s}^{\mathrm{disch}} \le p_{\max}^{\mathrm{disch}} u_{t,s}^{\mathrm{disch}} \tag{43}$$

Eqn. (41) shows that the actual power of the BESS at time *t* is equal to the discharging power minus the charging power. Eqns. (42) and (43) respectively show the minimum and maximum power limits of the charging and discharging power of the BESS.

2) Energy limits of a BESS.

$$E_{t+1,s}^{\mathrm{b}} = E_{t,s}^{\mathrm{b}} - \eta P_{t+1,s}^{\mathrm{b}} V_\mathrm{B} \quad \forall t = 0,...,T_\mathrm{B} - 1 \tag{44}$$

$$E_{\min}^{\mathrm{b}} \le E_{t,s}^{\mathrm{b}} \le E_{\max}^{\mathrm{b}} \quad \forall t = 0,...,T_\mathrm{B} \tag{45}$$

$$E_{0,s}^{\mathrm{b}} = \kappa E_{\mathrm{cap}}^{\mathrm{b}} \tag{46}$$

$$E_{T_\mathrm{B},s}^{\mathrm{b}} = E_{0,s}^{\mathrm{b}} \tag{47}$$

Eqn. (44) shows the energy transition equation of the BESS at different times. Eqn. (45) enforces that the energy of the BESS is within the upper and lower bounds. Eqn. (46) shows the initial energy of the BESS is κ times as much as its energy capacity. Eqn. (47) enforces that the energy of the BESS remains the same at the starting time and ending time of the restoration process.

3) Constraint of charging/discharging state.

$$u_{t,s}^{\mathrm{ch}} + u_{t,s}^{\mathrm{disch}} \le 1 \tag{48}$$

Eqn. (48) guarantees that the BESS cannot simultaneously charge and discharge.

4) Constraints of power outputs of the WF-BESS system.

$$P_{t,s}^{\mathrm{wb}} = P_{t,s}^{\mathrm{b}} + P_{t,s}^{\mathrm{w}} - P_{t,s}^{\mathrm{ab}} \tag{49}$$

$$0 \le P_{t,s}^{\mathrm{ab}} \le P_{t,s}^{\mathrm{w}} \tag{50}$$

Eqn. (49) shows the power output of the WF-BESS system is equal to the sum of the power output of the BESS and the WF minus the abandoned wind power. Eqn. (50) indicates the minimal and maximal limits of abandoned wind power.

5) Minimum charge/discharge time constraints. To reduce the number of charge/discharge cycles of energy storage units, the minimum charge/discharge constraints should be met [37]. Similar to the minimum up time constraints in unit commitment problems [29], the minimum charge time constraint is described as:

$$\sum_{t=1}^{T_{\mathrm{ch},1}} \left[1 - u_{t,s}^{\mathrm{ch}}\right] = 0 \tag{51}$$

$$\sum_{i=t}^{t+U_{\min}^{\mathrm{ch}}-1} u_{i,s}^{\mathrm{ch}} \ge U_{\min}^{\mathrm{ch}} y_{t,s}^{\mathrm{ch}},\ \forall t = T_{\mathrm{ch},1}+1,\cdots,T_{\mathrm{ch},2} \tag{52}$$

$$\sum_{i=t}^{T_\mathrm{B}} \left[u_{i,s}^{\mathrm{ch}} - y_{t,s}^{\mathrm{ch}}\right] \ge 0,\ \forall t = T_{\mathrm{ch},2}+1,\cdots,T_\mathrm{B} \tag{53}$$

where $T_{\mathrm{ch},1} = \min\left[T, (U_{\min}^{\mathrm{ch}} - U_0^{\mathrm{ch}})u_0^{\mathrm{ch}}\right]$, $T_{\mathrm{ch},2} = T - U_{\min}^{\mathrm{ch}} + 1$.

The minimum discharge time constraint is described as:

$$\sum_{t=1}^{T_{\mathrm{disch},1}} \left[1 - u_{t,s}^{\mathrm{disch}}\right] = 0 \tag{54}$$

$$\sum_{i=t}^{t+U_{\min}^{\mathrm{disch}}-1} u_{i,s}^{\mathrm{disch}} \ge U_{\min}^{\mathrm{disch}} y_{t,s}^{\mathrm{disch}},\ \forall t = T_{\mathrm{disch},1}+1,\cdots,T_{\mathrm{disch},2} \tag{55}$$

$$\sum_{i=t}^{T_\mathrm{B}} \left[u_{i,s}^{\mathrm{disch}} - y_{t,s}^{\mathrm{disch}}\right] \ge 0,\ \forall t = T_{\mathrm{disch},2}+1,\cdots,T_\mathrm{B} \tag{56}$$

where $T_{\mathrm{disch},1} = \min\left[T, (U_{\min}^{\mathrm{disch}} - U_0^{\mathrm{disch}})u_0^{\mathrm{disch}}\right]$, $T_{\mathrm{disch},2} = T - U_{\min}^{\mathrm{disch}} + 1$.

6) Logical relationship constraints of variables $y_{t,s}^{\mathrm{ch}}$ and $u_{t,s}^{\mathrm{ch}}$. The variable $y_{t,s}^{\mathrm{ch}}$ equals 1 if and only if $u_{t,s}^{\mathrm{ch}}$ equals 1 and $u_{t-1,s}^{\mathrm{ch}}$ equals 0, which is expressed as:

$$-(1 - y_{t,s}^{\mathrm{ch}})M < u_{t,s}^{\mathrm{ch}} - u_{t-1,s}^{\mathrm{ch}} \le y_{t,s}^{\mathrm{ch}} M \tag{57}$$

In the same way, the logical relationship constraint of variables $y_{t,s}^{\mathrm{disch}}$ and $u_{t,s}^{\mathrm{disch}}$ is expressed as:

$$-(1 - y_{t,s}^{\mathrm{disch}})M < u_{t,s}^{\mathrm{disch}} - u_{t-1,s}^{\mathrm{disch}} \le y_{t,s}^{\mathrm{disch}} M \tag{58}$$

7) Maximal fluctuation constraints of the combined power in contiguous time intervals.

$$-\gamma P_{\mathrm{rated}}^{\mathrm{w}} \le P_{t,s}^{\mathrm{wb}} - P_{t\text{-}1,s}^{\mathrm{wb}} \le \gamma P_{\mathrm{rated}}^{\mathrm{w}} \tag{59}$$

Eqn. (59) enforces that the ramp rate of scheduled wind power is between the upper and lower bounds.

8) Constraints of scheduled wind power for scenario s.

$$P_{t,s}^{\text{w,sch}} = \hat{P}_t^{\text{w,sch}}, \quad \lambda_{t,s} \tag{60}$$

Eqn. (60) shows that the scheduled wind power outputs for each scenario equal those attained in the RIM.

To sum up, the CSBESS can be formulated as

$$\begin{aligned} &Obj.\ (37) \\ &s.t.\ (38)-(60) \end{aligned} \tag{61}$$

V. Solution Method

A. Modification of T

Eqn. (3) shows that the value of T has a great impact on the restorability R_c. Due to the complexity and uncertainty of power system restoration procedures, exactly identifying the value of T is not easy, and therefore an estimation and modification method is proposed to determine the value of T.

At the initial stage, T is estimated based on the experience of system operators. When the generation curve of the power system is obtained by the RIM, the value of T can be modified. The restoration procedure is not assumed to terminate until all loads in the system are restored. t_{end} can be regarded as the minimal time point at which the active power of all units is larger than the sum of all loads, reserve power, and power losses, where the last two parts can be set as 8% of the total generated power [38]-[39].

$$t_{\text{end}} = \{\min t \mid \sum_{g \in \Omega_G} P_{g,t} \ge P_{\text{load}} + P_{\text{rev}} + P_{\text{loss}}\} \tag{62}$$

Therefore, the modified value of T is expressed as

$$T = t_{\text{end}} - t_{\text{st}} \tag{63}$$

Note that after T is modified, the RIM will be solved again based on the renewed T.

B. Solution Procedure

Benders decomposition is adopted to solve the proposed RIM-CSBESS coordination strategy. The RIM is regarded as the “master” problem, while the CSBESS serves as the “slave” problem. If the objective function of the CSBESS is not equal to zero, a generated cut (64) is added into the RIM.

$$W_s + \sum_{t=1}^{T_b} \lambda_{t,s} \left(P_{t,s}^{\text{w,sch}} - \hat{P}_t^{\text{w,sch}} \right) \le 0 \tag{64}$$

Both the RIM and CSBESS are formulated as MILP models and can be solved by high-performance commercial solvers. The flowchart of this solution method is as follows:

---

1. Estimate the value of T and input all parameter data.
2. Solve the RIM (34) based on the estimated T.
3. Modify the value of T through (63).
4. Solve the RIM (34) based on the updated T.
5. For any t, s:
   Solve the CSBESS (61). If objective (37) is not 0, generate a cut based on (64).
6. If all of the objectives of the CSBESS for different scenarios are 0, the algorithm terminates. Otherwise, aggregate the generated cuts and add them to the RIM, then return to step 2.

The proposed power system restoration strategy is based on two optimization problems that provide the mathematical foundations for the actual restoration planning. As long as each NBSU is restarted at its optimal starting time as indicated by the proposed method and the outputs of the WF-BESS are scheduled as optimized, the restorability of power systems can be improved in the actual restoration process. The effective performance of the proposed approach is illustrated by employing a case study of an actual power system in China, which is shown in Section VI.

VI. Simulation Results

A simulation test is implemented on a 64-bit personal computer with a 3.3 GHz CPU and 8 GB RAM. The algorithms are implemented in AMPL [40], and a highly efficient commercial solver CPLEX is employed to solve the models developed [41].

A. Test System Description

To demonstrate the effectiveness of the proposed method, its application to the Guangdong power system in China is presented. This partial network consists of 29 units, 163 nodes, and 212 transmission lines. The detailed topology is shown in Fig. 4.

The rated power of the wind turbine is 15 MW. The maximum ramp down rate and ramp up rate are -60 and 60 MW/h, respectively. The length of the time intervals for the RIM and CSBESS are 10 and 5 min, respectively. The restoration time of each transmission line is 5 min. The parameters of the WF and the BESS are shown in Table I. The BESS has been discharging for 15 min when the outage occurs. A total number of 10 representative scenarios of wind power outputs are employed.

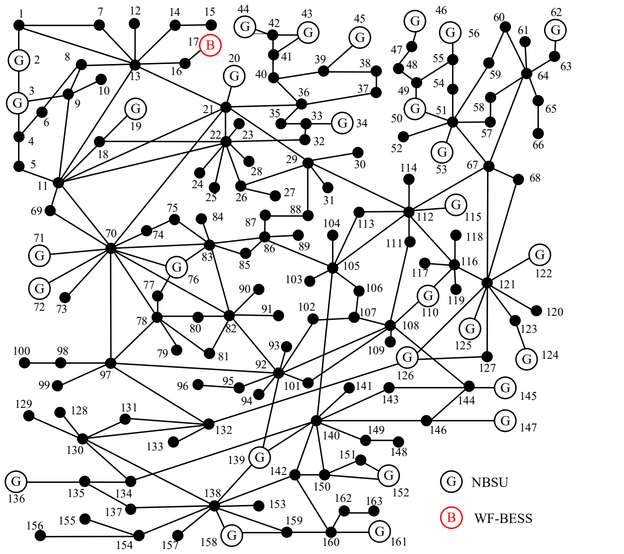

Fig. 4 Topology of the Guangdong power system in China employed in the case study.

B. Final Restoration Planning Determination

Using the proposed method, the maximum restorability is calculated, and the control strategy of the BESS for the studied network is created. The estimated value of T attained based on the experience of operators is 500 min. After the RIM is first solved, the value of T is modified to 220 min. After 21 iterations, the termination criterion is reached. The restorability of the power system is 2570.0 MW. Table II shows the optimal startup time stamps of all NBSUs. The Unit at bus 2 is the first to be started, and its starting time is at the 30$^{\text{th}}$ min.

C. Comparison of solutions by employing different methods

To illustrate the effectiveness of the proposed method, comparisons of power capacity achieved by employing the proposed method and the method in [30] are depicted in Fig. 5, where the red line represents the solutions attained by the proposed method. The total power capacity at the 220th min of the studied power system is 9102 MW, and the total energy capacity in the studied period is 9423.2 MWh. The black line represents the generation outputs attained by employing the method in [30], where the cranking time of NBSUs is fixed, based on a fixed cylinder temperature. The total power capacity at the 220th min attained by employing the method in [30] is 8804 MW, and the total energy capacity in the studied period is 9169.8 MWh. Fig. 5 shows that employing the proposed method results in a larger power capacity and total generated energy than the method in [30].

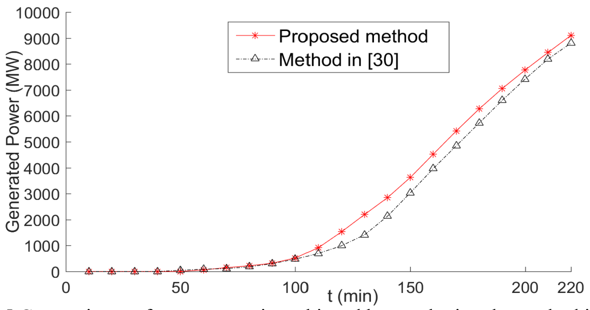

Fig. 5 Comparisons of power capacity achieved by employing the method in this paper and that in [30].

TABLE I
PARAMETERS OF THE WF-BESS IN CASE STUDY

WF data			
E_w^{min}	34.23 (MWh)	E_w^{max}	34.95 (MWh)
p_{wr}^-	-60 (MW/h)	p_{wr}^+	60 (MW/h)
P_{rated}^w	15 (MW)		
BESS data			
E_{min}^b	1 (MWh)	E_{max}^b	10 (MWh)
p_{max}^{disch}	10 (MW)	p_{max}^{ch}	10 (MW)
U_{min}^{ch}	25 (min)	U_{min}^{disch}	25 (min)
U_0^{ch}	0	U_0^{disch}	15 (min)
γ	0.6	β	0.1 (MW)
E_{cap}^b	11 (MWh)	κ	0.6
η	0.95		

TABLE II
STARTUP TIME OF NBSUS

No. of Units	19	3	53	44	45	122
Starting time/min	70	60	90	80	70	70
No. of Units	46	76	2	126	110	125
Starting time/min	70	60	30	70	60	60
No. of Units	56	50	147	152	43	158
Starting time/min	70	70	70	90	60	110
No. of Units	124	161	145	34	71	20
Starting time/min	90	80	80	40	60	80
No. of Units	72	62	115	139	136	
Starting time/min	90	110	90	80	60	

The solutions of the two strategies, i.e., the WF-BESS combined strategy and WF only strategy, are compared based on ten representative scenarios. The results of ten scenarios are given in Table III. By employing the WF only strategy, five scenarios have no solutions because the fluctuating wind power cannot provide sustainable cranking power for the NBSUs. With the aid of a BESS, the optimal solution can be attained for each scenario by employing the WF-BESS combined strategy. The approach is validated in Table III, which shows that the proposed WF-BESS combined restoration strategy can improve the restorability of power systems. Comparison of power capacity achieved by employing the WF-BESS combined strategy and WF only strategy based on Scenario 1 is shown in Fig. 6.

TABLE III
RESTORABILITY RESULTS OF THE WF-BESS COMBINED STRATEGY AND WF ONLY STRATEGY BASED ON TEN SCENARIOS (MW)

Scenarios	WF-BESS combined strategy	WF only strategy
1	2760.9	2420.3
2	2620.5	No solution
3	2612.7	No solution
4	2773.9	2589.2
5	2615.5	No solution
6	2600.0	No solution
7	2777.1	2567.5
8	2617.1	No solution
9	2735.0	2319.3
10	2725.7	2385.5

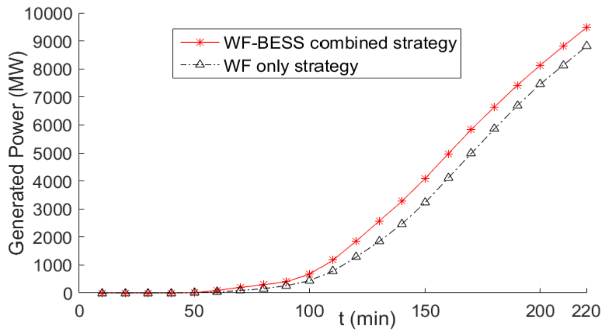

Fig. 6 Comparison of power capacity achieved by employing the WF-BESS combined strategy and WF only strategy based on Scenario 1.

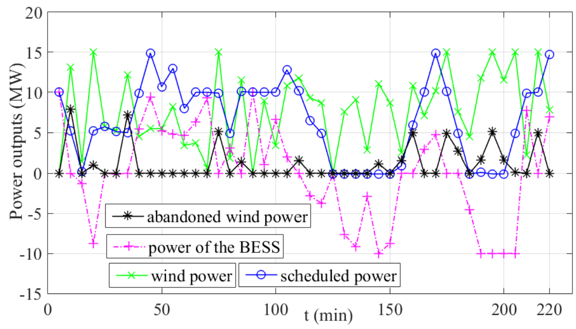

Fig. 7 Power outputs of the WF and BESS, scheduled wind power, and abandoned wind power in Scenario 8.

D. *Sensitivity Analysis*

Fig. 7 shows the power outputs of the WF and BESS, the scheduled wind power, and the abandoned wind power in Scenario 8 where the wind power output is the most volatile among all scenarios. The wind power outputs fluctuate violently in this scenario, and the BESS alternately charges and discharges to ensure that its energy can be flexibly dispatched. With limited abandoned wind power outputs, the power outputs of the WF-BESS system can meet the scheduled power.

Fig 8 shows the power outputs and energy capacity of the BESS in Scenario 8. The left axis indicates the power outputs of the BESS. The BESS is discharging if its power output is positive, and vice versa. The right axis indicates the energy capacity of the BESS. Due to the minimum charge/discharge time constraints, each charge state or discharge state lasts for at least 25 min.

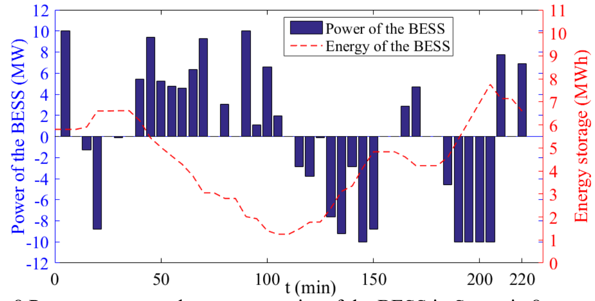

Fig. 8 Power outputs and energy capacity of the BESS in Scenario 8.

TABLE IV
RESTORABILITY RESULTS AND ITERATION NUMBERS FOR DIFFERENT BESS POWER CAPACITIES

Power capacity of the BESS (MW)	Restorability results (MW)	Iteration numbers
7	2328.7	36
8	2401.0	34
9	2401.0	21
10	2570.0	21
11	2584.7	11
12	2587.8	10
13	2607.1	8

TABLE V
RESTORABILITY RESULTS FOR DIFFERENT INITIAL STATE OF CHARGE OF THE BESS

Initial state of charge of the BESS	Restorability results (MW)
0.1	No solution
0.2	2384.0
0.4	2408.7
0.6	2570.0
0.8	2570.0
0.9	2570.0

TABLE VI
RESTORABILITY FOR SCENARIOS WITH DIFFERENT KANTOROVICH DISTANCES

Change in Kantorovich distance	Restorability results (MW)
-3%	2581.5
-2%	2578.8
-1%	2572.0
0	2570.0
+1%	2563.2
+2%	2544.9
+3%	2533.5

Table IV shows the restorability results and iteration numbers for different BESS power capacities. As the power capacity of the BESS increases, the restorability of the power system is improved. A BESS with a larger power capacity can respond to the demand for more power, and thus the starting time of NBSUs is shortened. Furthermore, the coordination between the RIM and CSBESS converges faster for larger BESS power capacities.

Table V shows the restorability results based on different initial states of charge of the BESS. It's seen from Table V that the restorability of the power system increases as the initial state of charge of the BESS increases. However, the restorability no longer increases once the initial state of charge of the BESS is larger than 0.6.

The impact of the uncertainty level of wind power outputs on the restorability is also investigated. In this work, the scenario analysis method is employed to address the uncertainty, and the uncertainty level is measured by the Kantorovich distance of selected representative scenarios [42]. The Kantorovich distance of employed scenarios in the case study is set as the reference value, and the scenarios with increased and decreased distances are employed to simulate the effect of the uncertainty level of wind power outputs on the restorability solutions, which is shown in Table VI. Table VI shows that the restorability result decreases as the Kantorovich distance of scenarios increases. When the uncertainty of wind power increases, the results are inclined to be conservative when taking scenarios with a larger Kantorovich distance into account, and therefore the restorability result decreases.

E. Computational Cost Analysis

Fig. 9 shows the changes in the power difference penalty between the scheduled power wind power outputs and the actual power outputs of the WF-BESS system with the increase in the number of iterations. After 21 iterations, the power difference is within the threshold. Therefore, the proposed method is verified as highly effective. The total computation time of the presented strategy for the actual power system is 2960.9 s, which is acceptable for restoration planning.

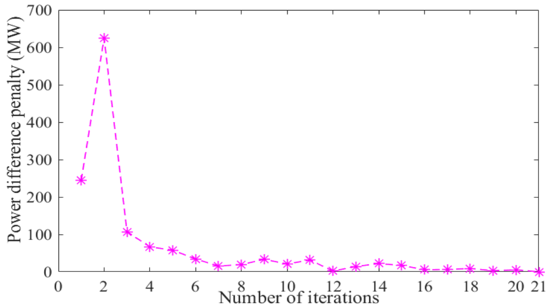

Fig. 9 Changes in the power difference penalty with increasing iteration number.

VII. CONCLUSION

This work investigated the positive contribution of a WF-BESS system to accelerating the restoration speed of power systems after outages. The concept of restorability is defined, and a restoration strategy for improving system restorability is proposed. The output of a WF is scheduled by a RIM model to provide active power to restart NBSUs. A BESS is employed and a CSBESS is developed to compensate for the volatile generation output of the WF so that the power outputs of the WF-BESS combined system can track the scheduled wind power optimized by the RIM. The performance of the proposed methodology is verified by simulations on the actual Guangdong power system. The simulation results indicate that the restorability of power systems can be significantly improved by employing the WF-BESS combined system. Moreover, the power capacity of BESSs greatly impacts the restorability improvement. Taking the uncertainty of wind power modeled by multiple scenarios into account, the proposed strategy demonstrates great potential for practical applications.

REFERENCES

[1] G. Liang, S. R. Weller, J. Zhao, F. Luo, and Z. Y. Dong, "The 2015 Ukraine blackout: implications for false data injection attacks," *IEEE Trans. Power Syst.*, vol. 32, no. 4, pp. 3317-3318, Jul. 2017.

[2] M. Nagpal, T. G. Martinich, Z. Jiao, S.-H. Manuel, H. A. Zhang, A. Alimardani, "Lessons learned from a regional system blackout and restoration in BC Hydro" *IEEE Trans. Power Delivery.*, vol. 33, no. 4, pp. 1954-1961, Aug. 2018.

[3] R. Yan, N. A. Masood, T. K. Saha, F. Bai, and H. Gu, "The anatomy of the 2016 South Australia blackout: A catastrophic event in a high renewable network," *IEEE Trans. Power Syst.*, vol. 33, no. 5, pp. 5374-5388, Sep. 2018.

[4] L. Sun, C. Peng, J. Hu, and Y. Hou, "Application of type 3 wind turbines for system restoration," *IEEE Trans. Power Syst.*, vol. 33, no. 3, pp. 3040-3051, May 2018.

[5] N. Goudarzi and W. D. Zhu, "A review on the development of wind turbine generators across the world," *Int. J. Dynam. Control*, vol. 1, no. 2, pp. 192-202, Jun. 2013.

[6] N. Ganganath, J. V. Wang, X. Xu, C. T. Cheng, and K. T. Chi, "Agglomerative clustering based network partitioning for parallel power system restoration," *IEEE Trans. Ind. Inf.,* vol. 14, no. 8, pp. 3325-3333, Aug. 2018.

[7] A. Golshani, W. Sun, Q. Zhou, Q. P. Zheng, and J. Tong, "Two-stage adaptive restoration decision support system for a self-healing power grid," *IEEE Trans. Ind. Inf.*, vol. 13, no. 6, pp. 2802-2812, Dec. 2017.

[8] F. Qiu and P. Li, "An integrated approach for power system restoration planning," *Proc. IEEE*, vol. 105, no. 7, pp. 1234-1252, Jul. 2017.

[9] A. Golshani, W. Sun and Q. Zhou, Q. P. Zheng, J. Wang, and F. Qiu, "Coordination of wind farm and pumped-storage hydro for a self-healing power grid," *IEEE Trans. Sustain. Energy*, vol. 9, no. 4, pp. 1910-1920, Oct. 2018.

[10] A. Golshani, W. Sun, Q. Zhou, Q. P. Zheng, and Y. Hou, "Incorporating wind energy in power system restoration planning," *IEEE Trans. Smart Grid*, early access, 2017.

[11] M. Aktarujjaman, M. A. Kashem, M. Negnevitsky, and G. Ledwich, "Black start with DFIG based distributed generation after major emergencies," 2006 *International Conference on Power Electronics, Drives and Energy Systems,* New Delhi, India, Dec. 12-15, 2006.

[12] R. Hu, W. Hu, P. Li, and C. Su, "A dynamic programming based method for optimizing power system restoration with high wind power penetration," *2016 IEEE 8th International Power Electronics and Motion Control Conference* (*IPEMC-ECCE Asia*), Hefei, China, May 22-26, 2016.

[13] Y. Xie, C. Liu, Q. Wu, K. Li, Q. Zhou, and M. Yin, "Optimized dispatch of wind farms with power control capability for power system restoration," *J. Mod. Power Syst. Clean Energy*, vol. 5, no. 6, pp. 908-916, Nov. 2017.

[14] G. He, Q. Chen, C. Kang, Q. Xia, and K. Poolla, "Cooperation of wind power and battery storage to provide frequency regulation in power markets," *IEEE Trans. Power Syst.*, vol. 32, no. 5, pp. 3559-3568, Sep. 2017.

[15] T. Zhao and Z. Ding, "Cooperative optimal control of battery energy storage system under wind uncertainties in a microgrid," *IEEE Trans. Power Syst.*, vol. 33, no. 2, pp. 2292-2300, Mar. 2018.

[16] S. Teleke, M. E. Baran, S. Bhattacharya, and A. Q. Huang, "Rule-based control of battery energy storage for dispatching intermittent renewable sources," *IEEE Trans. Sustain. Energy*, vol. 1, no. 3, pp. 117-124, Oct. 2010.

[17] X. Zhang, Y. Yuan, L. Hua, Y. Cao, and K. Qian, "On generation schedule tracking of wind farms with battery energy storage systems," *IEEE Trans. Sustain. Energy*, vol. 8, no. 1, pp. 341-353, Jan. 2017.

[18] S. Zhang, Y. Mishra and M. Shahidehpour, "Fuzzy-logic based frequency controller for wind farms augmented with energy storage systems," *IEEE Trans. Power Syst.*, vol. 31, no. 2, pp. 1595-1603, Mar. 2016.

[19] R. Dufo-López, J. L. Bernal-Agustín, and J. A. Domínguez-Navarro, "Generation management using batteries in wind farms: Economical and technical analysis for Spain," *Energy Policy*, vol. 37, no. 1, pp. 126-139, Jan. 2009.

[20] K. C. Divya and J. Østergaard, "Battery energy storage technology for power systems-an overview," *Electr. Pow. Sys. Res.*, vol. 79, no. 4, pp. 511-520, Apr. 2009.

[21] T. Chakraborty, D. Watson and M. Rodgers, "Automatic generation control using an energy storage system in a wind park," *IEEE Trans. Power Syst.*, vol. 33, no. 1, pp. 198-205, Jan. 2018.

[22] D. Watson, C. Hastie, B. Gaudette, and M. Rodgers, "Demonstrating stacked services of a battery in a wind R&D park," *IEEE Trans. Power Syst.*, vol. 33, no. 2, pp. 1411-1419, Mar. 2018.

[23] H. Yu, C. Y. Chung, K. P. Wong, H. W. Lee, and J. H. Zhang, "Probabilistic load flow evaluation with hybrid Latin hypercube sampling and Cholesky decomposition," *IEEE Trans. Power Syst*., vol. 24, no. 2, pp. 661-667, May 2009.

[24] J. Dupacova, N. Growe-Kuska, and W. Romisch, "Scenario reduction in stochastic programming: an approach using probability metrics," *Math. Program.*, vol. 95, no. 3, pp. 493-511, Mar. 2003.

[25] D. Watson, C. Hastie, and M. Rodgers, "Comparing different regulation offerings from a battery in a wind R&D park," *IEEE Trans. Power Syst.*, vol. 33, no. 3, pp. 2331-2338, May 2018.

[26] H. Bitaraf and S. Rahman, "Reducing curtailed wind energy through energy storage and demand response," *IEEE Trans. Sustain. Energy*, vol. 9, no. 1, pp. 228-236, Jan. 2018.

[27] Z. Li, M. Shahidehpour, F. Aminifar, A. Alabdulwahab, and Y. Al-Turki, "Networked microgrids for enhancing the power system resilience," *Proc. IEEE*, vol. 105, no. 7, pp. 1289-1310, Jul. 2017.

[28] M. Panteli, P. Mancarella, D. N. Trakas, E. Kyriakides, and N. D. Hatziargyriou, "Metrics and quantification of operational and infrastructure resilience in power systems," *IEEE Trans. Power Syst.*, vol. 32, no. 6, pp. 4732-4742, Nov. 2017.

[29] J. M. Arroyo and A. J. Conejo, "Optimal response of a thermal unit to an electricity spot market," *IEEE Trans. Power Syst.*, vol. 15, no. 3, pp. 1098-1104, Aug. 2000.

[30] W. Sun, C. C. Liu and L. Zhang, "Optimal generator start-up strategy for bulk power system restoration," *IEEE Trans. Power Syst*., vol. 26, no. 3, pp. 1357-1366, Aug. 2011.

[31] L. Sun, Z. Lin, Y. Xu, F. Wen, C. Zhang, and Y. Xue, "Optimal skeleton-network restoration considering generator start-up sequence and load pickup," *IEEE Trans. Smart Grid*, early access, 2018.

[32] X. Gu, W. Liu, and C. Sun, "Optimisation for unit restarting sequence considering decreasing trend of unit start-up efficiency after a power system blackout," *IET Gener. Transm. Distrib.*, vol. 10, no. 16, pp. 4187-4196, Aug. 2016.

[33] X. Dui, G. Zhu, and L. Yao, "Two-stage optimization of battery energy storage capacity to decrease wind power curtailment in grid-connected wind farms," *IEEE Trans. Power Syst.*, vol. 33, no. 3, pp. 3296-3305, May 2018.

[34] W. Yao, C. Y. Chung, F. Wen, M. Qin, and Y. Xue, "Scenario-based comprehensive expansion planning for distribution systems considering integration of plug-in electric vehicles," *IEEE Trans. Power Syst.*, vol. 31, no. 1, pp. 317-328, Jan. 2016.

[35] M. S. Modarresi, L. Xie, M. C. Campi, S. Garatti, A. Carè, A. A. Thatte, and P. R. Kumar, "Scenario-based economic dispatch with tunable risk levels in high-renewable power systems," *IEEE Trans. Power Syst.*, early access, 2018.

[36] T. K. A. Brekken, A. Yokochi, A. von Jouanne, Z. Z. Yen, H. M. Hapke, D. A. Halamay, "Optimal energy storage sizing and control for wind power applications," *IEEE Trans. Sustain. Energy*, vol. 2, no. 1, pp. 69-77, Jan. 2011.

[37] Q. Jiang, Y. Gong and H. Wang, "A battery energy storage system dual-layer control strategy for mitigating wind farm fluctuations," *IEEE Trans. Power Syst.*, vol. 28, no. 3, pp. 3263-3273, Aug. 2013.

[38] M. Milligan *et al.*, "Operating reserves and wind power integration: An international comparison," in *Proc. 9th Int. Workshop on Large-Scale Integration of Wind Power into Power Systems*, Quebec, Oct. 18–19, 2010.

[39] E. Benedict, T. Collins, D. Gotham, S. Hoffman, D. Karipides, S. Pekarek, and R. Ramabhadran, "Losses in electric power systems," Purdue University, Tech. Rep., 1992.

[40] R. Fourer, D. M. Gay, and B. W. Kernighan, "A modeling language for mathematical programming," *Manage. Sci.*, vol. 36, no. 5, pp. 519–554, May 1990.

[41] IBM Corp., IBM ILOG AMPL Version 12.2 User's Guide, 2010. Available: http://ampl.com/BOOKLETS/amplcplex122userguide.pdf.

[42] J. M. Morales, S. Pineda, A. J. Conejo, and M. Carrión, "Scenario reduction for futures market trading in electricity markets," *IEEE Trans. Power Syst.*, vol. 24, no. 2, pp. 878-888, May 2009.

Lei Sun received the B.Eng. degree from East China University of Science and Technology, Shanghai, China, in 2012, and the Ph.D. degree from Zhejiang University, Hangzhou, China, in 2017, both in electrical engineering.

He is currently a Lecturer in the School of Electrical Engineering and Automation, Hefei University of Technology, Hefei, China.

Weijia Liu received the B.Eng. and Ph.D. degrees in electrical engineering from Zhejiang University, Hangzhou, China, in 2011 and 2016, respectively.

He is currently a Postdoctoral Fellow in the Department of Electrical and Computer Engineering, University of Saskatchewan, Saskatoon, SK, Canada.

C. Y. Chung (M'01-SM'07-F'16) received the B.Eng. (with First Class Honors) and Ph.D. degrees in electrical engineering from The Hong Kong Polytechnic University, Hong Kong, China, in 1995 and 1999, respectively.

He is currently a Professor, the NSERC/SaskPower (Senior) Industrial Research Chair in Smart Grid Technologies, and the SaskPower Chair in Power Systems Engineering in the Department of Electrical and Computer Engineering at the University of Saskatchewan, Saskatoon, SK, Canada.

Dr. Chung is an Editor of *IEEE Transactions on Power Systems*, *IEEE Transactions on Sustainable Energ*y, and *IEEE Power Engineering Letters*. He is also an IEEE PES Distinguished Lecturer.

Ming Ding received the M.S. degree in electrical engineering from Xi'an Jiaotong University, Xi'an, China, in 1984.

He is a Doctoral Tutor and a Professor in the School of Electrical Engineering and Automation, Hefei University of Technology, Hefei, China. His research interests include power system reliability analysis, power system operation and planning, renewable energy, distributed generation, and FACTS.

Rui Bi received the B.S., M.S., and Ph.D. degrees from Hefei University of Technology in 2001, 2004, and 2016, respectively.

He is a Master's Tutor and a Lecturer in the School of Electrical Engineering and

Automation, Hefei University of Technology, Hefei, China. His research interests include power system operation and planning, renewable energy, distributed generation.

Linjie Wang received his B.Eng. degree in electrical engineering from East China University of Science and Technology, Shanghai, China, in 2012.

He is currently an engineer in Shangyu Power Supply Company, China.